

University of Groningen

Biochemical and structural insight into the chemical resistance and cofactor specificity of the formate dehydrogenase from *Starkeya novella*

Partipilo, Michele; Whittaker, Jacob J; Pontillo, Nicola; Coenradij, Jelmer; Herrmann, Andreas; Guskov, Albert; Slotboom, Dirk Jan

Published in:
The FEBS Journal

DOI:
[10.1111/febs.16871](https://doi.org/10.1111/febs.16871)

IMPORTANT NOTE: You are advised to consult the publisher's version (publisher's PDF) if you wish to cite from it. Please check the document version below.

Document Version
Publisher's PDF, also known as Version of record

Publication date:
2023

[Link to publication in University of Groningen/UMCG research database](#)

Citation for published version (APA):

Partipilo, M., Whittaker, J. J., Pontillo, N., Coenradij, J., Herrmann, A., Guskov, A., & Slotboom, D. J. (2023). Biochemical and structural insight into the chemical resistance and cofactor specificity of the formate dehydrogenase from *Starkeya novella*. *The FEBS Journal*, 290(17), 4238-4255. Advance online publication. <https://doi.org/10.1111/febs.16871>

Copyright

Other than for strictly personal use, it is not permitted to download or to forward/distribute the text or part of it without the consent of the author(s) and/or copyright holder(s), unless the work is under an open content license (like Creative Commons).




The publication may also be distributed here under the terms of Article 25fa of the Dutch Copyright Act, indicated by the "Taverne" license. More information can be found on the University of Groningen website: <https://www.rug.nl/library/open-access/self-archiving-pure/taverne-amendment>.

Take-down policy

If you believe that this document breaches copyright please contact us providing details, and we will remove access to the work immediately and investigate your claim.

Downloaded from the University of Groningen/UMCG research database (Pure): <http://www.rug.nl/research/portal>. For technical reasons the number of authors shown on this cover page is limited to 10 maximum.

Biochemical and structural insight into the chemical resistance and cofactor specificity of the formate dehydrogenase from *Starkeya novella*

Michele Partipilo¹ , Jacob J. Whittaker¹, Nicola Pontillo^{1,2}, Jelmer Coenradij¹, Andreas Herrmann^{2,3,4}, Albert Guskov¹  and Dirk Jan Slotboom¹ 

¹ Department of Biochemistry, Groningen Institute of Biomolecular Sciences & Biotechnology, University of Groningen, The Netherlands

² Polymer Chemistry and Bioengineering, Zernike Institute for Advanced Materials, Groningen, The Netherlands

³ DWI-Leibniz Institute for Interactive Materials, Aachen, Germany

⁴ Institute of Technical and Macromolecular Chemistry, RWTH Aachen University, Germany

Keywords

biocatalysis; cofactor regeneration; formate dehydrogenase; protein engineering; soil bacteria

Correspondence

D. J. Slotboom, Department of Biochemistry, Groningen Institute of Biomolecular Sciences & Biotechnology, University of Groningen, Nijenborgh 4, Groningen 9747 AG, The Netherlands
 Tel: +31 50 363 4187
 E-mail: d.j.slotboom@rug.nl

(Received 20 September 2022, revised 4 May 2023, accepted 19 May 2023)

doi:10.1111/febs.16871

Formate dehydrogenases (Fdhs) mediate the oxidation of formate to carbon dioxide and concomitant reduction of nicotinamide adenine dinucleotide (NAD⁺). The low cost of the substrate formate and importance of the product NADH as a cellular source of reducing power make this reaction attractive for biotechnological applications. However, the majority of Fdhs are sensitive to inactivation by thiol-modifying reagents. In this study, we report a chemically resistant Fdh (Fdh_{SNO}) from the soil bacterium *Starkeya novella* strictly specific for NAD⁺. We present its recombinant overproduction, purification and biochemical characterization. The mechanistic basis of chemical resistance was found to be a valine in position 255 (rather than a cysteine as in other Fdhs) preventing the inactivation by thiol-modifying compounds. To further improve the usefulness of Fdh_{SNO} as for generating reducing power, we rationally engineered the protein to reduce the coenzyme nicotinamide adenine dinucleotide phosphate (NADP⁺) with better catalytic efficiency than NAD⁺. The single mutation D221Q enabled the reduction of NADP⁺ with a catalytic efficiency k_{CAT}/K_M of 0.4 s⁻¹·mM⁻¹ at 200 mM formate, while a quadruple mutant (A198G/D221Q/H379K/S380V) resulted in a fivefold increase in catalytic efficiency for NADP⁺ compared with the single mutant. We determined the cofactor-bound structure of the quadruple mutant to gain mechanistic evidence behind the improved specificity for NADP⁺. Our efforts to unravel the key residues for the chemical resistance and cofactor specificity of Fdh_{SNO} may lead to wider use of this enzymatic group in a more sustainable (bio)manufacture of value-added chemicals, as for instance the biosynthesis of chiral compounds.

Abbreviations

ASA, accessible surface area; BME, 2-mercaptoethanol; CO₂, carbon dioxide; CV, column volume; DTNB, 5,5'-dithiobis-(2-nitrobenzoate); DTT, dithiothreitol; ECAA, ethyl 4-chloroacetoacetate; ECHB, ethyl (S)-(-)-4-chloro-3-hydroxybutyrate; EDTA, ethylenediaminetetraacetic acid dipotassium; Fdh, Formate dehydrogenase; GC content, guanine cytosine content; GQKV-Fdh_{SNO}, quadruple mutant of the formate dehydrogenase from *Starkeya novella* with the mutations A198G/D221Q/H379K/S380V; HMG-CoA, 3-hydroxy-3methylglutaryl-CoA; I_{C50} , inhibitory constant; IMAC, immobilized metal affinity chromatography; k_{CAT} , turnover number; K_M , Michaelis–Menten constant; KPi, potassium phosphate; LB, lysogeny broth; MgCl₂, magnesium chloride; MgSO₄, magnesium sulfate; MQ, Milli-Q water; MTSET, 2-(Trimethylammonium) ethyl methanethiosulfonate; N₃, azide; NaCl, sodium chloride; NAD⁺, nicotinamide adenine dinucleotide; NADP⁺, nicotinamide adenine dinucleotide phosphate; NEM, N-ethylmaleimide; PCMB, p-chloromercuribenzoate; PCR, polymerase chain reaction; PDB, Protein Data Bank; PEG, polyethylene glycol; SCN, thiocyanate; SDS/PAGE, Sodium-Dodecyl-Sulfate polyacrylamide gel electrophoresis; SEC, size exclusion chromatography; $t_{1/2}$, half-life value; T_m , melting temperature; WT, wild-type.

Introduction

Formate utilization is increasingly being explored as a sustainable alternative in the production of electricity and platform chemicals [1–4]. Low cost, high solubility, permeability to biomembranes and low reduction potential are among the main characteristics that make this C₁ compound one of the most attractive feedstocks for the development of ‘formatotrophic’ cell factories [5,6]. Micro-organisms that use formate as source of both carbon and reducing power must be equipped not only with a metabolism machinery for its assimilation (i.e. serine pathway or reductive acetyl-CoA pathway), but also with specific enzymes to exploit its reducing power, producing CO₂ as a waste product. The released carbon dioxide could then be electrochemically reduced back to formate, allowing to feed the biomanufacturing microbes in a continuous and circular manner [7].

NAD⁺-dependent formate dehydrogenases (Fdhs) (EC 1.17.1.9) [8] couple the oxidation of formate with the reduction of NAD⁺, producing CO₂ and NADH, which can be used for reductive metabolism. Fdhs from bacteria and methylotrophic yeasts have found applications for the regeneration of NADH *in vivo* [9–11], as well as *in vitro* [12–14]. Studies on the Fdh from *Pseudomonas* sp. 101 (Fdh_{PSE}) have laid the foundation for biochemical and mechanistic understanding of the enzyme family [15] and have been followed up by protein engineering efforts [12,16–20] to make Fdhs more effective biocatalysts for the large-scale production of optically active compounds [21–23]. However, Fdhs are well known for their sensitivity to chemical modification [15], which limits their potential use as regenerators of reduced redox cofactors in the field of biocatalysis. For instance, the α-haloketone substrates used in the reductive biosynthesis of α-halohydrins, which are important building blocks for

chiral compounds [24–26], inhibit Fdhs. In 2003, Hasegawa and collaborators reported the discovery of a native Fdh resistant to α-haloketones and thiol-modifying reagents, purified from *Thiobacillus* species, strain KNK65MA [27]. The chemical resistance of Fdh from *T. sp* KNK65MA (Fdh_{TBA}) was hypothesized to be caused by the presence of only five cysteines in the amino acid sequence instead of seven, as found in most of the bacterial Fdhs characterized so far (Table 1) [28]. The residues replacing the two ‘missing cysteines’ are a valine in position 255 and an alanine in position 288. The presence of a valine in position 255 indeed plays an important role in conferring high resistance to thiol reagents, as demonstrated by replacing Cys255 in Fdh_{PSE} [29]. The involvement of the residue in position 288 is less clear. Notably, the eukaryotic Fdhs from *Candida boidinii* (Fdh_{CBO}) and *Candida methylca* are also sensitive to thiol-modifying compounds as p-chloromercuribenzoate (PCMB) [30] and 5,5'-dithiobis-(2-nitrobenzoate) DTNB [31], but they lack a cysteine in the active site at the position corresponding to Cys255 in bacterial Fdhs. These yeast Fdhs have only two cysteines, which correspond to positions 52 and 288 in the bacterial enzymes.

In order to use Fdhs as effective NAD(P)H regenerators in biomanufacturing, it is necessary to unambiguously elucidate which cysteines are sensitive to chemical modifications, leading to protein inactivation. Here, we present the biochemical characterization of a novel NAD⁺-dependent formate dehydrogenase (Fdh_{SNO}) from the soil bacterium *Starkeya novella* recombinantly overproduced in *Escherichia coli* cells. Like its close homologue Fdh_{TBA}, Fdh_{SNO} exhibits a native resistance to thiol-modifying reagents. The protein has reduced sensitivity to inactivation to the α-haloketone ethyl 4-chloroacetoacetate (ECAA) (half-time of more than 4 h). We restored the missing

Table 1. Overview of the cysteine positions in the most studied Fdh-proteins. In the case of the yeast sequences from *C. boidinii* and *C. methylca*, the original position of the amino acids are reported in brackets. Positions 49 and 86 are also shown since they represent the main difference between the enzymes from *Thiobacillus* sp. KNK65MA and *Starkeya novella*.

Organism	Amino acid position										Total cysteines	Ref
	5	49	52	86	145	182	248	255	288	354		
<i>S. novella</i>	C	A	S	R	C	C	C	V	A	C	5	This study
<i>T. sp</i> KNK65MA	C	Q	S	K	C	C	C	V	A	C	5	[27]
<i>P. sp</i> 101	C	Q	S	R	C	C	C	C	C	C	7	[15]
<i>M. vaccae</i>	C	Q	S	R	C	C	C	C	C	C	7	[12]
<i>Mor. sp</i> C-1	C	A	S	K	C	C	C	C	C	C	7	[32]
<i>A. aquaticus</i>	C	Q	S	K	C	C	C	C	C	C	7	[33]
<i>C. boidinii</i>			C (23)						C (262)		2	[30]
<i>C. methylca</i>			C (23)						C (262)		2	[31]

The two ‘missing cysteines’ in positions 255 and 288 are highlighted in bold red.

cysteines in Fdh_{SNO} to establish the amino acids responsible for its chemical resistance. Crystallographic investigation of Fdh_{SNO} provides an insight into the functional characteristics of the chemical resistance, in comparison with the structures of known homologues. To make the enzyme also suitable for NADP⁺-dependent reactions, we investigated the effects of a single (D221Q) and quadruple mutant (A198G/D221Q/H379K/3380V), with the latter resulting in a better catalytic efficiency towards NADP⁺ than NAD⁺ as an electron acceptor. The cofactor-bound structure of the quadruple mutant Fdh_{SNO} offers a mechanistic explanation for the change in cofactor specificity.

Results

Gene overexpression and Fdh_{SNO} purification

To obtain an enzyme with improved chemical stability, we chose the gene *Snov_3272* encoding the formate dehydrogenase (Fdh_{SNO}, UniProt accession number: D7A8L2) from the genome of *Starkeya novella* DSM 506. The amino acid sequences of Fdh_{TBA} and Fdh_{SNO} differ only at positions 49 and 86, which play no role in either catalysis or substrate binding. Like Fdh_{TBA}, the *S. novella* enzyme contains only five cysteines instead of the seven cysteines usually found in homologues. It is the only annotated homologue of Fdh_{TBA} (among the available sequences with ≥80% identity) with the same reduced number of cysteines (Table S1).

The gene *Snov_3272* was initially cloned into an expression vector suitable for the recombinant overexpression in *E. coli*, but the high GC content [34] of the native gene from *S. novella* turned out to be incompatible with the codon usage of *E. coli* (Table S2). Thus,

we switched to a codon-optimized sequence of the gene (*synFdh*) for the expression in *E. coli* (a detailed analysis of the codon-optimization is available in Table S3 and Fig. S1). Fdh_{SNO} was then overproduced and isolated from the soluble fraction of *E. coli* MC 1061 [35] cells (as described in the Materials and Methods section), as evidenced by a band around 46 kDa on the Sodium-Dodecyl-Sulfate polyacrylamide gel (SDS/PAGE in Fig. 1A) in agreement with the calculated monomeric molar mass based on sequence. The protein was purified by a combination of immobilized metal affinity (IMAC) and size exclusion (SEC) chromatographies (Fig. 1B), with a reproducible yield around 90 mg of protein per litre of culture. The elution volume of the protein from the SEC corresponds to a mass of roughly 90 kDa, consistent with a dimeric state typical of bacterial Fdhs [15].

Biochemical characterization

We characterized the purified Fdh_{SNO} in terms of substrate specificity, inhibitor sensitivity, pH and temperature dependence, and stability. Fdh_{SNO} has one of the highest affinity for formate among known bacterial Fdhs [28], with a K_M value of 2.2 ± 0.4 mM (at an NAD⁺ concentration of 2.0 mM), and a k_{CAT} value of 0.9 s⁻¹. Fdh_{SNO} has a strong preference for NAD⁺ over NADP⁺. At a fixed concentration of 20.0 mM formate, the K_M for NAD⁺ was 115 ± 11 μM, and k_{CAT} 1.1 s⁻¹. We could not obtain kinetic values for NADP⁺ as an electron acceptor, although a marginal NADP⁺ reduction was observed using a large excess of the compound (Fig. S2).

Since the inhibitory capacity of small linear anions on NAD⁺-dependent Fdhs has been documented in the past

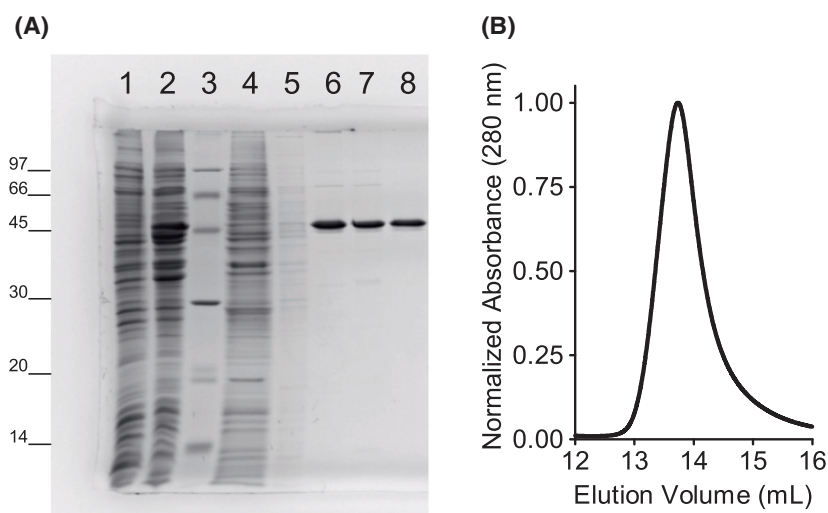


Fig. 1. Recombinant overproduction of Fdh_{SNO}. (A) SDS/PAGE of the purification steps. Lanes: 1 non-induced cells, 2 induced cells, 3 marker (the molecular weight of the bands is shown on the left, in kDa), 4 flow through of the IMAC column, 5 wash step of the IMAC column, 6 IMAC first fraction, 7 IMAC second fraction, 8 SEC fraction corresponding to the peak in B. (B) SEC profile resulting from the protein purification from 0.1 L culture of *E. coli* MC 1061 cells overproducing Fdh_{SNO}.

Table 2. Kinetic parameters of Fdh_{SNO}. In the case of formate and NAD⁺, the kinetic parameters come from biological quadruplicates ($n = 4$, the errors correspond to the standard deviation). For the inhibitory experiments, IC_{50} values are the average of biological triplicates ($n = 3$, the errors indicate s.e.m.). All the assays were carried out in 50 mM KPi at pH 7.5. N.D. stands for not determined in experimental conditions.

Compound	K_M (mM)	k_{CAT} (s ⁻¹)	IC_{50} (μM)	Co-substrate
Formate	2.2 ± 0.4	0.9 ± 0.0	–	2.0 mM NAD ⁺
NAD ⁺	0.1 ± 0.0	1.1 ± 0.0	–	20.0 mM Formate
NADP ⁺	N.D.	N.D.	–	50.0 mM Formate
Azide	–	–	0.1 ± 0.0	0.5 mM NAD ⁺ , 20.0 mM Formate
Thiocyanate	–	–	47.5 ± 11.4	0.5 mM NAD ⁺ , 20.0 mM Formate

[15], we verified their inhibitory potential and quantified the inhibitory constants (IC_{50}) of azide and thiocyanate (Fig. S3). We determined IC_{50} values of 100 nM for azide and 48 μM for thiocyanate. The kinetic parameters of Fdh_{SNO} are summarized in Table 2.

Next, we evaluated the effect of the pH on both enzymatic activity and protein stability. Fdh_{SNO} showed the highest activity around pH 7.5, but retained more than 70% of the maximal activity at a wide pH range (between 4.5 and 10.2 (Fig. 2A)). We tested the pH stability by incubating the protein for 20 h in different buffers (Fig. 2B), and found that potassium phosphate buffer at pH 7.5 was the best to preserve the protein activity. At pH values between 4.5 and 6.0, the enzymatic activity decreased over the 20 h incubation, but still between 50% and 75% of activity was retained. The incubation in carbonate (pH 9.2–10.2) and acetate at pH 4.0 led to the complete inactivation of Fdh_{SNO}.

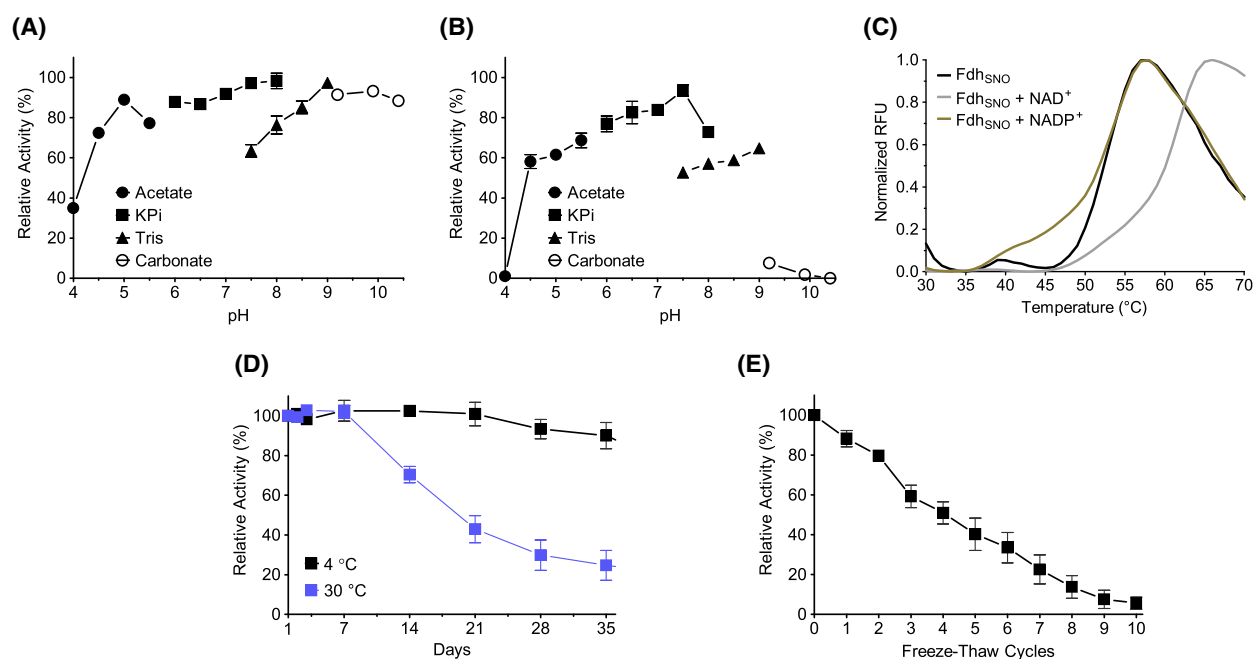


Fig. 2. Biochemical characterization of Fdh_{SNO}. Standard assay conditions are as follows: 0.2 μM Fdh_{SNO}, 0.5 mM NAD⁺, and 20 mM formate in 50 mM KPi, pH 7.5, at 30 °C. Error bars correspond to the s.e.m. between biological triplicates ($n = 3$). The activity of Fdh_{SNO} under standard assay conditions is arbitrarily set to 100% and it is intended as initial velocity during the first minute of reaction, unless stated otherwise. (A) Effect of pH on activity. The protein activity was tested in the presence of 100 mM buffers (● acetate at pH 4.0–5.5, ■ KPi at pH 6.0–8.0, ▲ Tris at pH 7.0–9.0, ○ carbonate–bicarbonate at pH 9.2–10.4). (B) Effect of pH on stability. Upon 20 h of incubation at 30 °C at different pH (100 mM buffers), the activity was evaluated under standard assay conditions. (C) Thermal shift assay of Fdh_{SNO} in the presence of NAD⁺ and NADP⁺. The fluorescence in terms of normalized relative fluorescent units (RFU) of the dye SYPRO Orange was monitored as a function of the temperature, revealing the binding to Fdh_{SNO} (5 μM) when protein denaturation occurred. The graph shows the average of experiments carried out in quadruple technical replicates without (black line) and with 10 mM NAD⁺ (grey line) or 10 mM NADP⁺ (brown line). (D, E) Influence of the temperature (D) and the number of freeze–thaw cycles (E) during protein storage on activity. The initial velocities after the first day of storage at the chosen temperature (4 °C in black and 30 °C in blue), or in the absence of freeze–thaw cycles represent 100% activity.

The melting temperature (T_m) of Fdh_{SNO} in the absence of any nicotinamide cofactor was estimated by thermal shift assay at 52.5 °C (Fig. 2C), which agrees well with the T_m measured for Fdh_{TBA} [27]. As expected, the addition of NADP⁺ barely affected the protein T_m ($T_{m, NADP^+} = 53.5$ °C), while the presence of NAD⁺ led to an increase in T_m of nine degrees ($T_{m, NAD^+} = 61.5$ °C), confirming binding and thus the strict specificity of Fdh_{SNO} towards NAD⁺.

Storage at 4 °C preserved activity over long time-scales, with 90% activity retained after 35 days of storage in the fridge (Fig. 2D, black line). At 30 °C, Fdh_{SNO} remained close to be fully active over the first week of storage (blue line). Freeze–thaw cycles (Fig. 2E) had a larger inactivating effect on Fdh_{SNO}, with a linear loss of activity as a function of the number of freeze–thaw cycles, consistent with cold denaturation of the purified protein progressively taking place, as reported for numerous other enzymes [36].

Restoration of sensitivity to thiol-modifying reagents by mutagenesis

We tested the effect of thiol reagents on activity (Fig. 3A,B) by incubating the protein for 2 min prior to the start of the reaction by the addition of formate. We chose a set of chemicals with different charges, sizes and binding mechanisms: n-ethylmaleimide (NEM), PCMB, 2-(Trimethylammonium)ethyl methanethiosulfonate (MTSET) and 5,5'-dithiobis-(2-nitrobenzoate) (DTNB). We also tested the effect of the reducing agents dithiothreitol (DTT) and 2-mercaptoethanol (BME), which we used to ensure that Fdh_{SNO} did not undergo detrimental oxidation events during the purification and storage procedures. Both DTT and BME slightly improved the protein activity, respectively, to 107% and 114%. As predicted based on the sequence, Fdh_{SNO} was resistant to inactivation by the thiol-modifying reagents, retaining most of its activity in the presence of NEM (87%), MTSET (81%) and DTNB (79%). PCMB was the only exception, as it caused a decrease of the activity to 27%. Likely, interactions take place with side chains of other amino acids than cysteine (imidazole and carboxylic groups), which are prone to form complexes with organomercurial compounds [37,38], affecting the protein functionality.

In order to get more detailed insight into the amino acids responsible for the chemical resistance, we compared the cysteines present in Fdh_{SNO} with those in the homologous bacterial and eukaryotic Fdhs reported as sensitive to NEM, DTNB and PCMB (Table 1). Besides the valine in position 255 and the alanine in position

288 that distinguish the chemically resistant Fdh_{SNO} and Fdh_{TBA}, we also tested position 52 which is occupied by serine in Fdh_{SNO}, whereas thiol-sensitive Fdhs in yeast species have a cysteine (C23 in the native sequence). In these eukaryotic Fdhs, only two cysteines are part of the monomeric sequence, and intriguingly the other cysteine is not located at the position equivalent to 255 in the bacterial enzymes, but instead is found at position 288 (natively C262).

We purified to homogeneity single mutants of Fdh_{SNO} introducing cysteines at positions 52, 255 and 288 in order to 'restore' susceptibility to thiol-reagents (Fig. S4). For each mutant, we evaluated the effect of reducing agents (DTT and BME), azide, thiocyanate and thiol-modifying reagents (Fig. 3B). The activity of the three mutants did not show significant changes from that of the wild-type (WT) in the presence of DTT and BME. Also the inhibition mediated by azide and thiocyanate remained unaltered in the mutants. In contrast, the cysteine restoration in position 255 caused susceptibility to thiol reagents, leading to complete protein inactivation upon incubation with 2.0 mM MTSET and 0.2 mM PCMB, and almost complete inhibition with 2.0 mM NEM or 0.2 mM DTNB (residual activity of 3%). Instead, S52C and A288C retained the resistance to all tested thiol-modifying reagents, showing no difference with the wild-type Fdh_{SNO}. Since only V255C displayed the loss in chemical resistance, we proceeded to quantify its chemical stability by longer incubations with the thiol compounds (Table 3, time courses in Fig. 3C), and compared it with the WT Fdh_{SNO}. As expected, the half-life values ($t_{1/2}$) of V255C for all the tested thiol-reagents were lower than 1 min (circles in Fig. 3C). In contrast, the chemical stability of the WT protein (squares in Fig. 3C) proved to be higher than V255C, albeit to a variable extent that depended on the specific compound.

Due to the potential use of Fdhs in the synthesis of valuable organic building-blocks, we also assessed the activity of Fdh_{SNO} and its cysteine mutants in the presence of ECAA and ethyl (S)-(–)-4-chloro-3-hydroxybutyrate (ECHB), as shown in Fig. 3D,E. Both the α -haloketone and α -haloalcohol are precursors to statins, a broad class of HMG-CoA (3-hydroxy-3methylglutaryl-CoA) reductase inhibitors for lowering blood cholesterol [39,40]. As with the thiol reagents, the activity of WT Fdh_{SNO} was not significantly affected by either 20 mM ECAA or ECHB. This chemical resistance was similarly conserved also in the S52C and A288C mutants, but the restoration of the cysteine in position 255 led to a drop in activity in the presence of ECAA, with only 20% residual activity compared with the wild-type upon

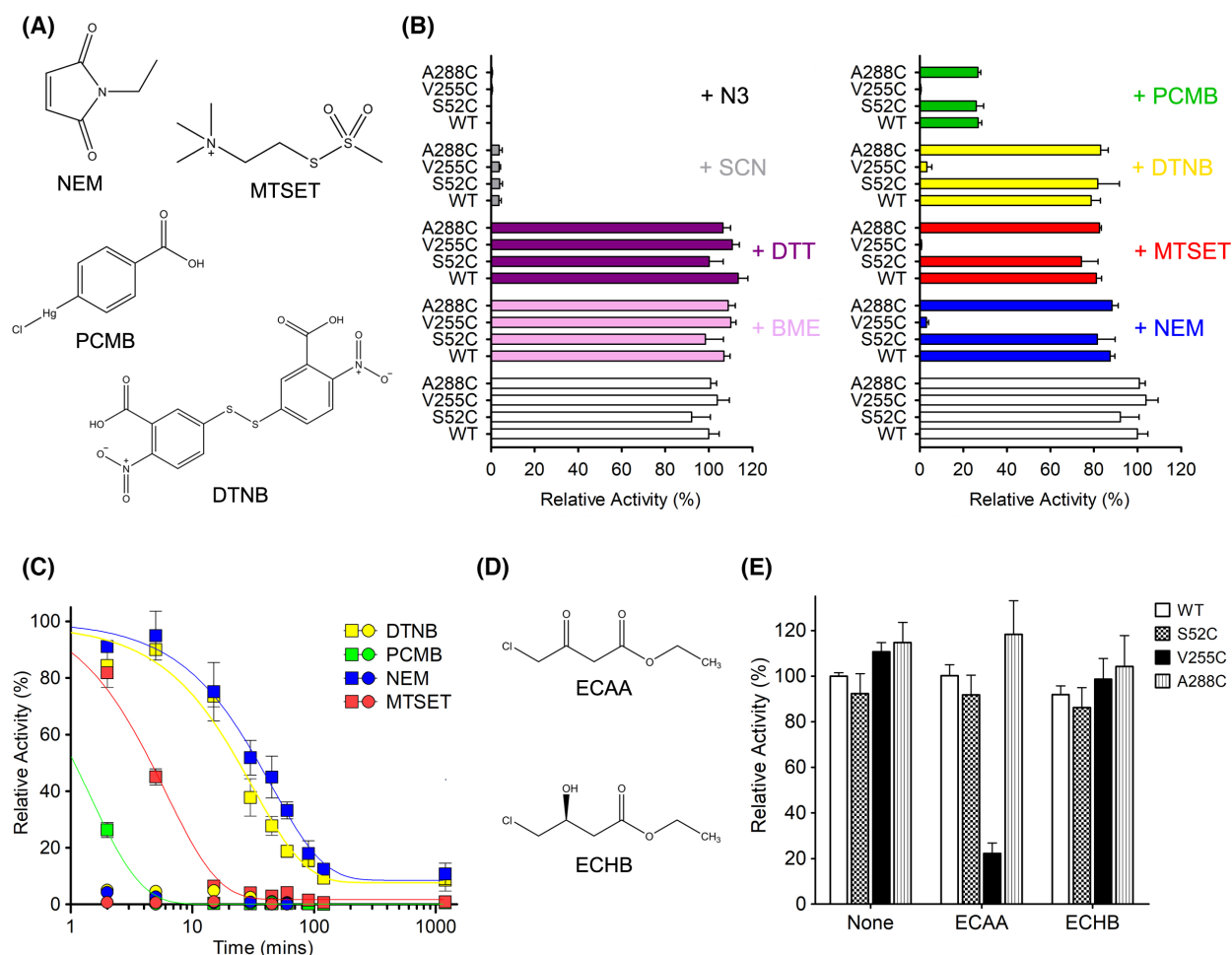


Fig. 3. Thiol-resistance of Fdh_{SNO}. (A) Structures of the thiol reagents NEM, MTSET (2-(Trimethylammonium)ethyl methanethiosulfonate), PCMB and DTNB (5,5'-dithiobis-(2-nitrobenzoate)). (B) Effects of thiol-reagents on the activity of the native Fdh_{SNO} and its cysteine mutants upon 2 min incubation. The initial rate of reaction of the native enzyme in the absence of any compound (white bars) was set to 100% activity. The conditions including the reducing agents BME and DTT are shown in pink and purple, respectively. The activity in the presence of the thiol-modifying compounds NEM, MTSET and DTNB and PCMB is respectively reported in blue, red, yellow and green, while in the case of the small linear anions azide (N3) and thiocyanate (SCN) is highlighted in black and grey, respectively. BME, DTT, NEM, MTSET, SCN and N3 were used at the concentration of 2.0 mM, while DTNB and PCMB at 0.2 mM. The assays were carried out under standard assay conditions in biological triplicates ($n = 3$, the s.e.m. is shown in the error bars). (C) Chemical stability against thiol-reagents of WT Fdh_{SNO} (squares) and V255C (circles). In both cases, 100% activity was set as the initial velocity of the enzymatic reaction in the absence of the thiol-reagents. At the chosen time point, the incubated protein (at 25 °C) was tested under standard assay conditions. The data comes from biological triplicates ($n = 3$), the error bars indicate the s.e.m. The concentrations of the thiol-compounds were the same of fig. B. (D) Structures of the α -haloketones ECAA and ECHB. (E) Effects of ECAA and ECHB on the activity of Fdh_{SNO} cysteine-restored variants. Following an incubation of 2 min, the protein activities were tested in the absence or in the presence of 20 mM α -haloketones (ECAA or ECHB). Data comes from three independent measurements ($n = 3$) under standard assay conditions, reporting the s.e.m. as error bars.

2 min incubation. The V255C sensitivity to ECAA was also evident from the estimation of the half-life value (~ 1 min). By contrast, the chemical stability of WT Fdh_{SNO} against the α -haloketone was 300 times higher than V255C, with a $t_{1/2}$ of almost 5 h (Table 3). The wild-type enzyme was even more resistant to inactivation by ECHB, for which we could not calculate a $t_{1/2}$ value even after 24-h incubation (Fig. S5). Replacing

Val255 with a cysteine made instead the enzyme susceptible to the α -haloalcohol ($t_{1/2} \sim 45$ min).

Structural insight into the chemical resistant Fdh_{SNO}

To gain further insights into the functional features of Fdh_{SNO}, we solved the crystal structure of the

Table 3. Half-time values ($t_{1/2}$) of the Fdh_{SNO} activity for the thiol-modifying reagents employed in this study. The data come from biological triplicates ($n = 3$, the errors are reported as standard deviation). N.Q. means “not quantifiable”, as the protein inactivation was complete in less than a minute. N.D. stands for “not determined” after 24 h incubation.

Compound	Concentration (mM)	$t_{1/2}$ (min)	
		WT	V255C
PCMB	0.2	1 ± 0	N.Q.
MTSET	2.0	4 ± 1	N.Q.
DTNB	0.2	22 ± 10	N.Q.
NEM	2.0	31 ± 17	N.Q.
ECAA	20.0	284 ± 105	N.Q.
ECHB	20.0	N.D.	46 ± 9

apoenzyme to a resolution of 2.1 Å (PDB entry 7QZ1, more details in the [Materials and Methods](#) section). Crystallographic data and refinement statistics are summarized in Table S4.

Like its structurally characterized homologues (summarized in Table S5), Fdh_{SNO} forms a homodimeric assembly of two identical monomers (Fig. 4A). Each monomer consists of two domains that adopt the Rossmann fold, a structural motif typical of nucleotide binding proteins [41]. Upon structural superimposition of the structures of Fdh_{SNO} and Fdh_{PSE} in complex with NAD⁺ (PDB entry 2NAD), it was possible to

identify the binding site of NAD⁺. The main amino acids involved in the binding of the cofactor are Ala198, Asp221, Val255 and Ser380, as highlighted in Fig. 4B.

By comparison with the structure of homologues sensitive to thiol reagents, FDH_{SNO} shows no major reorganization in the secondary or tertiary structure, as shown in the right panel of Fig. 4A. In all of the positions under examination (residues 52, 255 and 288), the orientation of the side chains remained unchanged, regardless of the presence of the thiol of the cysteine or of the specific substituent group (hydroxyl in Ser52, isopropyl in Val255, methyl in Ala288). Moreover, the mutations do not affect the accessible surface area (ASA) of each of these residues (Table S6). Val255 was more exposed to the solvent (highest ASA) than Ala288 and Ser52, which have little-to-no ASA for solvent. Val255 was the only residue to be located in the coenzyme binding pocket. Its proximity with the NAD⁺ binding site explains why the residue in this position plays a critical role in allowing or preventing the cofactor binding when a thiol-modifying reagent is present.

Cofactor specificity can be changed by mutations

Because numerous enzymes with industrial biomanufacturing potential (e.g. cytochrome P450 and

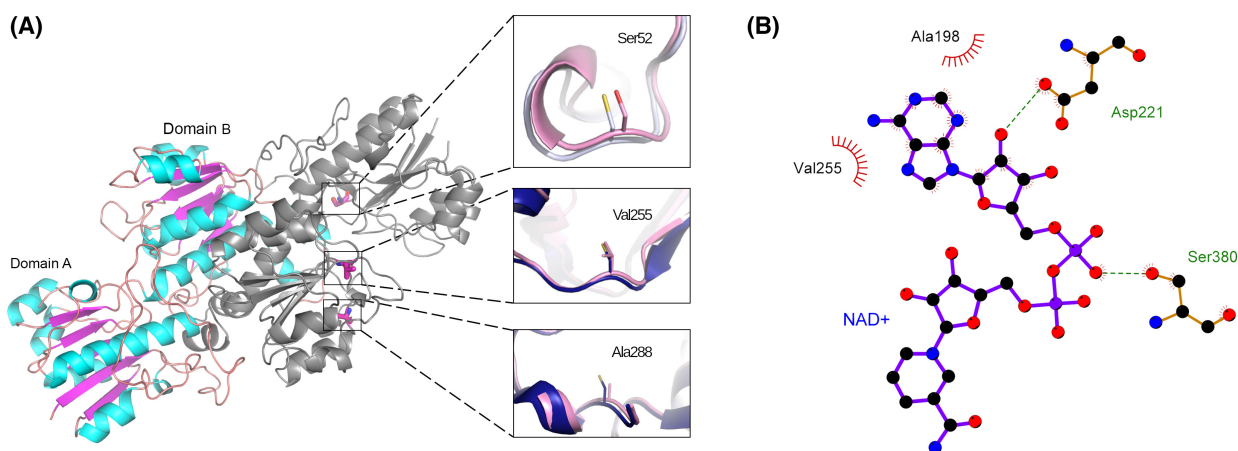


Fig. 4. Structural insight in Fdh_{SNO}. (A) Cartoon representation of the homodimeric assembly oriented alongside the two-fold axis. The two domains (domain A and domain B in the coloured monomer) present in each monomer adopt Rossmann folds, of which helices and strands are respectively highlighted in cyan and magenta. The three enlarged parts on the right show the superimposition of S52, V255 and A288 (PDB: 7QZ1, RMSD 1.10 Å) with the Fdh homologues containing cysteines in the same position (PDB: 2NAC for position 255 and 288, PDB: 5DNA for position 52). The image was generated by UCSF CHIMERA 1.4 software. (B) Diagram of the main interactions for the binding of NAD⁺ in Fdh_{SNO}. The binding site was identified by superimposition of chain A of Fdh_{SNO} and chain A of Fdh_{PSE} in complex with NAD⁺ (PDB: 2NAD). The analysis of the two structures reveals hydrogen bonds involving D221 and S380 (dashed lines) with different moieties of the cofactor, a hydrophobic interaction of V255 with the adenine ring and a stabilizing role of A198 for the correct orientation of D221. Such stabilization is mediated by the carbonyl group of A198 that sterically constraints the orientation of the adjacent A199 (not shown), which forms the hydrogen bond with D221 [42].

cyclohexanone monooxygenases) require NADPH rather than NADH as a cofactor [43,44], we decided to explore the possibility to change the co-substrate specificity of Fdh_{SNO}. An NADP⁺-variant of this chemically resistant Fdh may be coupled with NADPH-dependent biocatalytic processes to provide regeneration of the expensive NADPH by oxidation of formate. We selected the point mutation D221Q and the quadruple mutation A198G/D221Q/H379K/S380V (GQKV-Fdh_{SNO} from now on). The neutralization of the negative charge of Asp221 has long been known to change the coenzyme specificity [45,46]. The other three mutations were chosen by combining the main interactions observed with the cofactor from our superimposed crystallographic structure (Fig. 4B) with the observations from other studies on NADP⁺-dependent Fdhs [20,47,48].

We determined the kinetic parameters of the purified D221Q and GQKV mutants (SEC profiles in Fig. S6), for NAD⁺, NADP⁺ and formate in the presence of both the cofactors (Table 4, see Fig. S7 for the graphs).

D221Q Fdh_{SNO} acquired the ability to reduce NADP⁺ in addition to NAD⁺, with an 11-fold lower K_M for the phosphorylated cofactor (K_M of 0.3 mM for NADP⁺, 3.3 mM for NAD⁺). At the same time, the affinity of the mutant for formate in the presence of NAD⁺ was more than doubled (K_M of 5.5 mM) compared with the WT enzyme. Therefore, we conclude that the substitution of aspartate 221 with glutamine leads to broadened specificity with both NAD⁺ and NADP⁺ tolerated as electron acceptors, at the expense of the affinity for NAD⁺.

The quadruple mutant GQKV showed a twofold increase in k_{CAT} compared to D221Q when NADP⁺ and formate are cosubstrates, and even a better affinity

for NADP⁺ resulting in a K_M value of 0.1 mM that practically matches the one for NAD⁺ in WT Fdh_{SNO}. The three additional mutations did not alter the K_M for formate in the presence of NADP⁺ (15.6 mM for GQKV, 16.7 mM for D221Q), but NAD⁺ became a poorer substrate for the GQKV variant, as not only the K_M for NAD⁺ was doubled compared with D221Q, but also the affinity for formate (K_M of 22.1 mM) increased fourfold with NAD⁺ as a co-substrate. Finally, the improvement of the quadruple mutant over the single one for the change of specificity appears evident in terms of catalytic efficiency: the k_{CAT}/K_M for NADP⁺ was five times higher than D221Q.

A structural insight into the NADP⁺ dependency of GQKV-Fdh_{SNO}

To further understand the effect of the chosen mutations on cofactor specificity, we determined the crystallographic structure of GQKV-Fdh_{SNO} in complex with NADP⁺ and azide at a resolution of 2.5 Å (Fig. 5A–E and Table S4, PDB entry 8OQ2). To assess any structural differences, the quadruple mutant was compared against the cofactor-bound structure of the closest homologue specific for NAD⁺, namely FDH_{PSE} (PDB entry 2NAD).

The replacement of Ala198 with a glycine (Fig. 5B) enlarged the pocket accommodating the nicotinamide adenosine ring, resulting in the loss of a direct interaction between the cofactor and the amino acid side chain (4.14 Å distance between the oxygen atom of the ribose ring and the α -carbon atom of Gly198 in the mutant Fdh, vs 2.74 Å between the main oxygen of the ribose ring and the side chain carbon of Ala198 in FDH_{PSE}).

Table 4. Kinetic parameters of the NADP⁺-dependent Fdh_{SNO} constructs. The values were obtained from independent triplicates ($n = 3$), the errors represent the s.e.m. N.D. not determined.

Fdh _{SNO} construct	Substrate	K_M (mM)	k_{CAT} (s ⁻¹)	k_{CAT}/K_M (s ⁻¹ ·mM ⁻¹)	Co-substrate
Wild type	Formate _{NAD}	2.2 ± 0.4	0.9 ± 0.0	0.4 ± 0.0	2.0 mM NAD ⁺
	NAD ⁺	0.1 ± 0.0	1.1 ± 0.0	9.8 ± 0.3	20.0 mM Formate
	Formate _{NADP}	N.D.	N.D.	N.D.	–
	NADP ⁺	N.D.	N.D.	N.D.	–
D221Q	Formate _{NAD}	5.5 ± 1.6	0.1 ± 0.0	0.0 ± 0.0	20.0 mM NAD ⁺
	NAD ⁺	3.3 ± 1.3	0.2 ± 0.0	0.0 ± 0.0	350.0 mM Formate
	Formate _{NADP}	16.7 ± 2.6	0.1 ± 0.0	0.0 ± 0.0	3.0 mM NADP ⁺
	NADP ⁺	0.3 ± 0.1	0.1 ± 0.0	0.4 ± 0.0	200.0 mM Formate
GQKV (A198G/D221Q/H379K/S380V)	Formate _{NAD}	22.1 ± 3.0	0.2 ± 0.0	0.0 ± 0.0	20.0 mM NAD ⁺
	NAD ⁺	6.4 ± 1.3	0.2 ± 0.0	0.0 ± 0.0	350.0 mM Formate
	Formate _{NADP}	15.6 ± 2.2	0.2 ± 0.0	0.0 ± 0.0	3.0 mM NADP ⁺
	NADP ⁺	0.1 ± 0.01	0.2 ± 0.0	1.9 ± 0.1	200.0 mM Formate

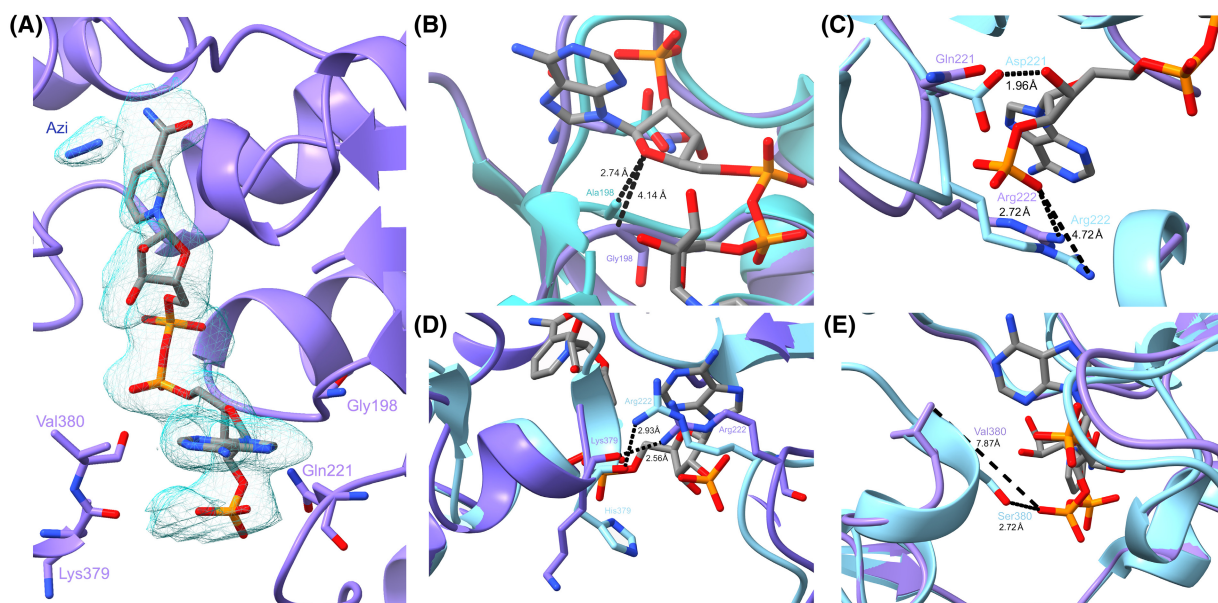


Fig. 5. Structural basis for NADP⁺-specificity of GQKV-Fdh_{SNO}. (A) The binding-site of GQKV-Fdh_{SNO} in the presence of NADP⁺ and azide (The $2F_o - F_c$ electron density map is contoured at a sigma level of 1.2. RMSD of 1.35 Å). (B–E) Zoom into the specific mutations A198G (B), D221Q (C), H379K (D) and S380V (E). The NADP⁺-bound structure of GQKV-Fdh_{SNO} (PDB entry 80Q2) is highlighted in purple, while the superimposed NAD⁺-bound structure of Fdh_{PSE} (95% similarity with Fdh_{SNO}) is reported in cyan. All the panels were prepared with UCSF CHIMERAX version 1.4.

Asp221 plays a key role in the NAD⁺ dependency of Fdh_s by establishing hydrogen bonds with the hydroxyl groups in positions 2'- and 3'- of the ribose moiety, and electrostatically repelling the negative phosphate substituent of the NADP⁺ cofactor. Neutralizing aspartate by mutation to glutamine (Fig. 5C) allowed NADP⁺ recognition as a preferred co-substrate. Besides, the insertion of Gln221 led to the distinct reorientation of the side chain of the adjacent arginine in position 222, enabling not only the formation of a salt-bridge interaction with the 2'-phosphate group of NADP⁺, but also a further hydrogen bond with the N1 atom of the adenosyl ring.

The introduction of Lys379 did not seem to establish a direct interaction with the cofactor (Fig. 5D); however, a closer proximity with one of the terminal amines of Arg222 (2.56 Å) was observed in contrast with His379 in the NAD⁺-bound structure (2.93 Å): this might suggest a stabilizing function in the favour of the specific reduction of NADP⁺.

Following the point mutation S380V, a reorientation of the side chain was observed in comparison with the Fdh_{PSE} structure. Within the homologue structure, the hydroxyl group of Ser380 points directly towards the unoccupied binding site and is separated by 2.72 Å from the closest phosphate group of the nicotinamide pyrophosphate. In contrast, the mutation to Val380

leads to a near 180° flip in the side chain position while the orientation of the amino acid backbone remains largely unchanged. The backbone hydroxyl group is now the closest moiety to the same phosphate, whereas the Val380 side chain is 7.87 Å from the phosphate, enabling an opening of over 5 Å at this location of the binding site. The mutation of S380V does not represent a significant steric alteration to promote or inhibit the binding of substrate; however, it is likely that the extremely polar NADP⁺ substrate would have a repulsive influence on the hydrophobic valine side chain, yielding this reorientation of side chain positioning.

Discussion

Starkeya novella is known for its extensive metabolic flexibility, since it is a mesophilic organism able to grow not only on single carbon compounds (such as methanol and formate) and sulfur derivatives (e.g. thiosulfate) [49], but also in soils contaminated with toxic organophosphate insecticides [50] and organic fuel additives [51]. Bacteria that survive a variety of environmental stresses from extreme natural conditions to artificial pollutants, could harbour valuable biocatalysts for the manufacture of platform chemicals [52,53]. Thus, the rich diversity in soil prokaryotic

communities [54,55] represents a promising source to explore for a new arsenal of enzymes for (bio)chemical syntheses [56,57].

In this study, we report the isolation and characterization of a novel chemically resistant Fdh encoded by the soil bacterium *S. novella*. Fdh_{SNO} displayed similar kinetic parameters to the previously characterized bacterial Fdhs [28], with a K_M for formate in the low millimolar range and a strict dependence on NAD⁺, for which the affinity lies in the micromolar range. In particular, the K_M value for formate of 2.2 mM is one of the most favourable affinity constants among Fdhs, around 3–7 times lower than the characterized homologues from *Pseudomonas* sp.101, *Mycobacterium vaccae* N10 and *C. boidinii*. On the contrary, the k_{CAT} around 1/s is lower than to the values in Fdh_{PSE} and Fdh_{CBO}, respectively, with a k_{CAT} of 7/s and 4/s. The biochemical characteristics of Fdh_{SNO} match well with those of the other characterized Fdhs [28]: high activity in a wide pH range (4.5–10.2), an optimum temperature around 50 °C and good storage capacity at 4 °C. Fdh_{SNO} gradually loses activity when subjected to multiple rounds of freezing and thawing, a procedure often used to deliver enzymes into the lumen of liposomes.

Azide was found to be a powerful Fdh_{SNO} inhibitor, with an estimated IC_{50} of 10^{-7} M, four orders of magnitude lower than the K_M for formate (10^{-3} M). This means that traces of azide (commonly used in the range of 0.02–0.1%, corresponding to 5×10^{-3} M – 2.5×10^{-2} M, as an antimicrobial agent [58]) in reagents and equipment that will come into contact with Fdh need to be carefully removed to prevent protein inhibition. Crystal structures of bacterial Fdhs (including the quadruple mutant of Fdh_{SNO} reported in this work) co-crystallized with NAD(P)⁺ and azide (Fig. S8) reveal that the azide molecule forms a dense network of hydrogen bonds with Ile122, Asn146, Arg284 and His332 in the active site. These interactions lead to the formation of a protein conformation analogous to the one adopted in the transition state during formate conversion [59]. Although thiocyanate shares with azide the characteristics of a three-atom linear anion, it is 500 times less effective as an inhibitor. In the absence of a structure of the ternary complex with the cofactor and thiocyanate, we speculate that thiocyanate is less suitable to form hydrogen bonds with the aforementioned residues, probably because hydrogen bond formation with the molecule is more sensitive to the relative orientation of the bond donor, and due to the lower electronegativity of the sulfur atom compared to the nitrogen atoms of azide. Hence, the restricted ability of the sulfur atom to coordinate hydrogen bonds with donors leads to a weaker inhibition than the triatomic nitrogen compound [60].

Since we observed that Fdh_{SNO} is chemically resistant to various thiol-modifying compounds, we designed ‘cysteine-restoring’ mutants in those positions suspected to lead to sensitivity [27]. We tested the mutations S52C and A288C corresponding to the only cysteines present in homologous Fdhs in *Candida* species, which were reported as sensitive to compounds with high affinity for thiol groups [30,31]. In addition, Slusarczyk and coworkers highlighted how replacing these cysteines in Ser52 (C52S) and Ala288 (C288A) resulted in a four- to fivefold increase in resistance to Cu²⁺ ions [17]. We also introduced a cysteine at position 255, of which the oxidation or the chemical modification is the main cause of chemical inactivation of the enzyme [15]. Our work pinpoints that the presence of a valine at position 255 is responsible for the chemical resistance of Fdh_{SNO}, with no measurable roles of Ser52 and Ala288. This experimental conclusion is reinforced by the crystal structure. The residue at position 255 is located in the cofactor-binding pocket in the proximity of the adenine part without directly participating in the catalytic action [42]. Upon mutation of Val255 into a cysteine, the thiol group of Cys255 is accessible to thiol-modifying reagents. Steric hindrance resulting from the cysteine modification prevents the binding of the cofactor, culminating in protein inhibition. Therefore, the absence of the thiol group in Fdh_{SNO} represents the key feature underlying the chemical resistance of this enzyme. Valine and cysteine display similar ASAs to the solvent in position 255 (Table S6); consequently, the different chemistry between the thiol and the isopropyl groups seems to be the only relevant determinant. The amino acids at positions 52 and 288 are both too distant from the active site and not accessible enough to the solvent to play an effective role in the chemical resistance mechanism.

The increased resistance of Fdh_{SNO} against the alpha-halo compounds ECAA and ECHB, and the thiol-modifying reagents NEM, DTNB, MTSET and PCMB makes the enzyme a more versatile long-lasting supplier of reducing power for industrial biomanufacturing. It may be possible to boost the stability of Fdh_{SNO} further. Strategies for increasing the operational stability of Fdhs have been reviewed elsewhere [8,28].

With improved chemical resistance, Fdh_{SNO} also is an ideal template to change the specificity for NAD⁺ into NADP⁺ in order to make a flexible toolset of enzymes for regeneration of the reduced cofactor of choice. The single mutation of aspartate at position 221 into glutamine was found to allow the reduction of NADP⁺, while maintaining the ability to convert

NAD⁺ into NADH, albeit with a 30 times lower affinity than the WT enzyme. In order to obtain a NADP⁺-dependent version of Fdh_{SNO} with better catalytic efficiency, we selected the mutations of the amino acids in positions 379 and 380, similarly to the recent work described by Calzadiaz-Ramirez *et al.* [20]; the role of Gly198 in altering the K_M values for the cofactors was already known, as it minimizes the steric hindrance to accommodate the phosphate group in position 2' of the ribose ring belonging to NADP⁺ [18,20]. Together with A198G and D221Q, the replacements H379K and S380V have been identified as 'epistatic mutations' that act synergistically to improve both the affinity and the turnover number for NADP⁺. In particular, His379 is known to stabilize the stacking of the adenosine moiety of NAD⁺, while Ser380 binds the pyrophosphate group in the proximity of the adenine ribose [42]. The occurrence of a lysine instead of histidine was previously observed in the Fdh-homologue from *Granulicella mallensis* MP5ACTX8, which displayed double cofactor specificity with a preference for NADP⁺ [48]. Its structure in complex with the cofactor revealed how the presence of Lys379 disrupts any possible interaction with the adenosine moiety, as the side chain of the amino acid is directed towards the solvent rather than the substrate: our structure confirmed this observation and further suggested a possible stronger interaction with Arg222 (Fig. 5D). On the other hand, the substitution S380V introduces a side chain that cannot interact anymore with the nicotinamide pyrophosphate, but that allows the steric accommodation of the phosphate group indicative of NADP⁺. The result of these synergistic mutations can explain the higher catalytic efficiency for NADP⁺ of our GQKV-Fdh_{SNO} compared with the single mutant D221Q Fdh_{SNO}, as well as the worsening of the K_M value for both the substrates when NAD⁺ is the co-substrate.

In conclusion, unlike multisubunit Fdh complexes containing iron–sulfur clusters and various metal ions [61,62], NAD⁺-dependent Fdhs are versatile enzymes that do not require a prosthetic group to produce NADH or NADPH from formic acid, releasing CO₂ as a final product. With a minimal mutagenic approach of a chemically resistant Fdh specific for NAD⁺ (Fdh_{SNO}), we highlighted the residues critical to modulate the specificity for NAD⁺ and NADP⁺. Wild-type or mutant enzymes can be chosen to regenerate NAD(P)H, depending on the requirement of the specific cofactor or of the intermediates formed in the biosynthesis process of interest, taking advantage of the oxidation of the low-cost chemical formate.

Particularly, Fdh_{SNO} has recently been successfully used as a pivotal component of a minimal enzymatic pathway triggered by formate ensuring the redox regeneration in the field of bottom-up synthetic biology [14,63]. Furthermore, the manufacture of valuable enantiomers for different industries [25] could represent an application for this biocatalyst, both in *in vivo* and *in vitro* systems. The compatibility of chemically resistant Fdhs in productive processes has already been shown with the precursors of statins [12], encouraging the use of such enzymes for pathways whose synthetic steps have the same chemistry, such as adrenergic receptor agonists or selective serotonin reuptake inhibitors [64–66]. Likewise, Fdh_{SNO} could prove to be a suitable tool for enzymatic or microbial bioremediation of sites contaminated by chemical and metal pollutants [67–69], avoiding the exhaustion of the reduced cofactor pool that supports the biodegradation process. Alternatively, the biochemically and structurally explored mutations on Fdh_{SNO} could be applied to high turnover number Fdh-homologues to combine catalytic efficiency, chemical resistance and desired cofactor specificity.

Materials and methods

Chemicals

Common chemicals for *in vivo* and *in vitro* procedures were purchased at the highest purity grade available from Carl Roth GmbH & Co. KG, Karlsruhe, Germany, or Merck KGaA. The thiol-reagents DTT (DTT-RO, CAS 3483-12-3), BME (M6250, CAS 60-24-2), NEM (E3876, CAS 128-53-0), DTNB (322123, CAS 69-78-3), ECAA (180769, CAS 638-07-3), ECHB (460524, CAS 86728-85-0) were purchased from Merck KGaA, Darmstadt, Germany. MTSET (91021, CAS 155450-08-1) was obtained from Biotium Inc., Fremont, CA, USA.

Bioinformatic analysis

The screening of the homologues of Fdh_{TBA} (UniProt accession number: Q76EB7) was carried out with the HMMER web service (<https://www.ebi.ac.uk/Tools/hmmer/>). Once Fdh_{SNO} was identified as the target protein, we obtained the encoding sequence by inquiring the Genome Database Collection BioCyc (<https://biocyc.org/>).

The numbers referring to the codon bias of the microorganisms *Starkeya novella* DSM 506 and *E. coli* K-12 (Table S2) are publicly available from the online resource (<https://www.kazusa.or.jp/codon/>) of the Kazusa DNA Research Institute [70].

Accessible surface area of amino acids (Table S6) was estimated using the 'Accessible Surface Area and

Accessibility Calculation for Protein' version 1.2 provided by the Center for Informational Biology, Ochanomizu University (<http://cib.cf.ocha.ac.jp/bitool/ASA/>).

Expression plasmid construction

The native gene of the Fdhs *Snov_3272* (https://bacteria.ensembl.org/Starkeya_novella_dsm_506_gca_000092925/Gene/Summary?g=Snov_3272;r=Chromosome:3436073-3437278;t=ADH90546) was PCR-amplified using the primers snofdh001 and snofdh002 (all the primers used in this study are listed in Table S7), while the template was constituted by the genomic-DNA of *Starkeya novella* purchased from the DSMZ collection (DSM 506). The codon-optimized version of the same gene (*synfdh*) for the expression in *E. coli* was designed and then acquired on the 'Gene Art gene synthesis' portal (Thermo Fisher Scientific, Inc., Waltham, MA, USA), which provided the synthetic gene into the pMA-RQ cloning vector. This plasmid was used as template for the PCR-amplification by the primers snofdh003 and snofdh004. Both the PCR-products *Snov_3272* and *synfdh* were consequently cloned first in the pINIT vector and then in the expression plasmid pBXC3H of the FX cloning kit [71], as previously described [14]. For the purpose of selection of the correct plasmid sequences, *E. coli* MC1061 cells (ATCC® 53338) [35] were used. The resulting constructs were verified by DNA-sequencing.

Site-directed mutagenesis

The introduction of the single mutations S52C, V255C, A288C and D221Q was made according to the protocol of the QuikChange Site-Directed Mutagenesis Kit (Agilent Technologies, Inc., Santa Clara, CA, USA). The primers employed for the construction of each mutant are reported in Table S7. As pBXC3H_ynfdh was the selected vector for the gene overexpression, we adopted it as DNA-template for the mutagenic PCR. Following the amplification in 50 μ L as the final volume, each reaction mixture was treated with the restriction enzyme DpnI (10 U· μ L⁻¹) to digest the parental non-mutated DNA for 1 h at 37 °C. 5 μ L of the digestion mixture was used to transform MC1061 chemocompetent cells by heat shock. The successful outcome of the site-directed mutagenesis was assessed by sequencing the isolated plasmids. The construction of the quadruple mutant GQKV was carried out similarly to the single mutants, but starting from pBXC3H_ynfdhD221Q as template for a double round of site-directed mutagenesis. We first inserted the single mutation A198G using the primers snofdh011 and snofdh012, obtaining the vector pBXC3H_ynfdhA198GD221Q. After verifying the correct insertion of the second mutation, we repeated the PCR-mutagenesis procedure using the double mutant vector (pBXC3H_ynfdhA198GD221Q) as a template, amplifying the DNA with the primers snofdh015 and snofdh016. Also in this case, the

resulting vector pBXC3H_ynfdhA198GD221QH379KS380V was confirmed by sequencing.

Protein overproduction and purification

Fdh from *Starkeya novella* was overproduced in MC1061 *E. coli* cells as heterologous host, similarly to what was previously described [14]. Briefly, the pBXC3H_ynfdh strain was grown at 37 °C, 200 rpm, in LB medium + 100 μ g·mL⁻¹ ampicillin, up to the optical density \cong 0.6, to be then induced with final 0.01% v/v L-arabinose. Following the induction, the culture was moved at 20 °C and left overnight shaking at 200 rpm. Around 20 h after the arabinose addition, the cells were spun down (15 min, 6000 g, 4 °C), and washed with buffer A (50 mM KPi pH 7.5, 150 mM NaCl), centrifuging with the same parameters. The resulting pellet was resuspended in an approximate volume of 30 mL buffer A, supplementing it with 100 μ g·mL⁻¹ DNase, 1 mM MgSO₄, 1 mM phenylmethylsulfonyl fluoride, to be consequently sonicated for 10 min (3 s on, 6 s off cycle, 70% amplitude) using a VCX130 Vibra-Cell sonicator (Sonics & Materials, Inc., Newton, CT), keeping the sample chilled over the cell disruption. After adding 1 mM -K-EDTA pH 7.0, the insoluble fraction was removed by further centrifugation at 48 254 g, 4 °C for 30 min, while the supernatant was flash-frozen with liquid nitrogen to be stored at -80 °C.

At the moment of the protein purification, the cytosolic fraction was quickly thawed and incubated in a Econo-Pac column (Bio-Rad Laboratories, Inc., Hercules, CA, USA) for 30 min at 4 °C with 1 mL of Ni²⁺-Sepharose resin (Ni Sepharose® 6 Fast Flow Cytiva) and 10 mM imidazole pH 7.5, on continuous shaking. The resin material was pre-washed with 20 column volumes (CV) MQ and 20 CV buffer A. After the incubation, the soluble fraction was left flowing through by gravity, leaving the His-tagged enzyme trapped in the nickel resin. Then, the resin material was washed with 20 CV buffer A + 50 mM imidazole pH 7.5, and eventually the bound protein was eluted in several fractions of buffer A + 500 mM imidazole pH 7.5 (the first fraction corresponded to 70% of the packed CV, the sequential ones to 50% CV). The fractions containing the protein were pooled, centrifuged for 5 min at 21 230 g, 4 °C with EDTA 1.0 mM, pH 7.0, and loaded on a Superdex 200 Increase 10/300 GL column (GE Healthcare, Chicago, Illinois, USA), attached to a NGC Quest™ 10 Chromatography System (Bio-Rad Laboratories, Inc.) with an incorporated UV detector. The protein was eluted with buffer A and its concentration was assessed afterwards spectrophotometrically (NanoDrop Technologies, Inc., Wilmington, DE, USA) using the extinction coefficient (ϵ_{280} nm = 62 340 M⁻¹·cm⁻¹) calculated with the online tool ProtParam (<https://web.expasy.org/protparam/>). Last, Fdh_{SNO} was concentrated on a 10 kDa centrifugal filter device Amicon® Ultra 0.5 mL (Merck Millipore Ltd.,

Darmstadt, Germany) to 2–4 mg·mL⁻¹, supplemented with 10% glycerol (v/v) and stored at –80 °C, after flash-freezing aliquots of 60–80 µL. As further controls of the different protein isolation steps, we harvested several fractions over the purification process for the SDS/PAGE (Fig. 1A) and eventually loaded them on SDS blots made of a 15% separating gel and a 5% stacking gel.

The same protocol for the protein overproduction and the purification was used for the S52C, V255C, A288C, D221Q and GQKV mutants.

Activity and kinetic assays

The activity of Fdh_{SNO} and its mutants was monitored following the reduction of NAD(P)⁺ at 340 nm ($\epsilon_{\text{NAD(P)H}}$, 340 nm = 6.22 mm⁻¹·cm⁻¹) in a SPARK 10 M plate reader (Tecan) at 30 °C. The standard assay conditions include in the reaction mixture 50 mM KPi pH 7.5, 0.2 µM Fdh_{SNO}, 0.5 mM NAD⁺ and 20 mM formate. All the biochemical assays shown in Fig. 2A–E were performed on biological triplicates ($n = 3$, the error bars represent the s.e.m.) coming from different purification batches, unless differently stated.

The effect of different pH and buffers was evaluated in terms of activity and stability using 100 mM acetate (pH 4.0–5.5), KPi (pH 6.0–8.0), Tris (pH 7.0–9.0) and carbonate (pH 9.2–10.4). 100% activity was represented in both cases by the initial velocity obtained by the condition of 100 mM KPi at pH 7.5. For the pH activity experiments (Fig. 2A), the standard assay conditions were modified employing 0.3 mM NAD⁺. In the pH stability set-up (Fig. 2B), the incubation of the protein with the buffer of choice was carried out for 20 h at 30 °C. After that, the mixture was transferred in the 96-well plates, final 0.5 mM NAD⁺ was added and the reaction was started upon the addition of 20 mM sodium formate.

The T_m of Fdh_{SNO} (Fig. 2C) was determined in the presence and absence of NAD⁺ and NADP⁺ substrates using the SYPRO Orange method [72]. The optimal protein:dye ratio was found after initial screening tests by varying the ratios of protein (1–20 µM) and dye (1–10×) in the presence of 50 mM KPi, pH 7.5. The experiments in the presence of the cofactors were carried employing the final nicotinamide concentration of 10 mM. In 96-well PCR plates, the apo-, NAD⁺- and NADP⁺-Fdh_{SNO} conditions were prepared in technical quadruplicates starting from 50 µM protein in buffer supplemented with 5× SYPRO Orange dye. Each sample was directly diluted in the wells with MQ water to obtain final 5 µM protein, and then resuspended. The T_m experiments were performed using a BioRad iCycler iQ instrument by measuring at the wavelength of 575 nm. A temperature range of 25–95 °C was chosen with a dwell time of 1 min between each datapoint collected.

To determine the influence of the temperature storage (Fig. 2D), 3.0 µM Fdh_{SNO} aliquots were conserved in the dark at 4 and 30 °C. For each time point, part of these

aliquots was used at the final concentration of 0.3 µM in standard assay conditions.

The effect of several freeze–thaw cycles (Fig. 2E) was assessed in standard assay conditions, following the flash-freezing in liquid nitrogen and consequent rapid thawing in a 10 °C water bath of 2.0 µM Fdh_{SNO} aliquots.

The kinetic parameters of the wild-type Fdh_{SNO} were spectrophotometrically determined in 50 mM KPi pH 7.5, at 30 °C, as previously described [14], using 0.2 µM enzyme. In short, keeping the NAD⁺ concentration constant at 2.0 mM, we calculated the micromoles of NADH formed per minute per milligram of protein by adding different amounts of formic acid (0.3–18.0 mM). By varying the NAD⁺ concentration from 10 to 1000 µM, we estimated the kinetics for the cofactor by adding 20 mM formic acid. Measurements were made in quadruplicate ($n = 4$, the error indicates the standard deviation) and the corresponding initial velocities were fitted through the Michaelis–Menten equation. In the case of the NADP⁺-specific variants of Fdh_{SNO} D221Q and GQKV (A198G/D221Q/H379K/S380V), we fixed NADP⁺ at 3.0 mM and added the range of 0.3–200.0 mM sodium formate to start the reactions. To calculate the kinetic parameters for NADP⁺, variable amounts of cofactor (10–3000 µM) were employed keeping the formate concentration constant at 200 mM. In the presence of NAD⁺, we changed the range of formate to 1–350 mM, while the amount of NAD⁺ was fixed at 20 mM. Vice versa, we estimated the kinetic parameters for NAD⁺ (0.25–40.0 mM) adding the constant concentration of 350 mM sodium formate for both the mutants. The kinetics of Fdh_{SNO} D221Q and GQKV are the result of measurements on biological triplicates ($n = 3$, the errors correspond to the s.e.m.), plotted according to the Michaelis–Menten model (Fig. S7).

In the IC₅₀ experiments (Fig. S3), we incubated the inhibitors with the mixture reaction for a few min before adding the formate to start the assay under standard conditions. Azide was tested in the 10⁻¹ to 10⁻⁸ mM range, while thiocyanate was used in the 10⁻⁵ to 10² mM range. The relative activity for each condition was determined by comparison with the initial velocity displayed by Fdh_{SNO} in the absence of the inhibitor (arbitrarily set at 100%).

Thiol-resistance and stability experiments

The experiments shown on Fig. 3B,E on Fdh_{SNO} WT and its cysteine mutants S52C, V255C, A288C were carried out at 30 °C, as described in the above-mentioned standard assay conditions, including 50 mM KPi pH 7.5, 0.2 µM Fdh_{SNO}, 0.5 mM NAD⁺ and 20 mM formate. All the thiol compounds used were freshly prepared, since they were solubilized in 50 mM KPi pH 7.5 buffer and immediately added to the reaction mixture. After 2 min of incubation with the nicotinamide cofactor and the enzyme, formate was added to trigger the reaction, which was

spectrophotometrically monitored at 340 nm. BME, DTT, NEM and MTSET were used at the final concentration of 2.0 mM, while DTNB and PCMB were tested at the final concentration of 0.2 mM. DTNB was freshly prepared and stored in an eppendorf tube covered with aluminium foil to prevent photo-damage events [73]. PCMB was solubilized according to the procedure described for p-mercuribenzoates by KK Han *et al.* [74]. In the case of ECAA and ECHB, we diluted them directly in 50 mM KPi pH 7.5 buffer at the concentration of 200 mM, and finally tested at 20 mM in the same manner described for the other thiol compounds.

The chemical stability experiments (Table 3, Fig. 3C and Fig. S5) were measured under standard assay conditions, in the same operational way of the other activity assays. 2.0 μ M Fdh_{SNO} (WT and V255C) was incubated at 25 °C with the chosen thiol-reagent in a 1 : 1 mixture (respectively, 2.0 mM DTNB, 2.0 mM PCMB, 20.0 mM NEM, 20.0 mM MTSET, 200 mM ECAA, 200 mM ECHB). At the time point of interest, 40 μ L of the mixture containing the protein and thiol compound (thus their final concentrations are 10 times lower in the enzymatic assay) were added to 150 μ L solution (130 μ L 50 mM KPi pH 7.5 and 20 μ L of 5.0 mM NAD⁺), mixed and 10 μ L of 400 mM sodium formate (20 mM final) were then added to trigger the enzymatic reaction in 200 μ L of final volume. Setting the initial velocity in the absence of any compound as 100% relative activity, we plotted the obtained initial velocities using the one-phase decay equation built-in in the GRAPHPAD PRISM software to calculate the protein half-life ($t_{1/2}$) for each tested compound.

Crystallization conditions and data collection

In order to prepare the protein for crystallographic purposes, the overproduction and purification procedures were carried out as described above, with the only exception being the elution buffer during SEC, which was composed of 20 mM HEPES pH 7.0, 50 mM NaCl. Upon initial screening with commercial kits, Fdh_{SNO} was crystallized using the hanging-drop vapour diffusion technique. An equal volume (1 μ L) of apo-protein solution (12 mg·mL⁻¹) was mixed with the crystallization solution [0.1 M Bis-Tris pH 5.5, 5–20% polyethylene glycol (PEG) 3350, 0.1 M MgCl₂] and allowed to equilibrate at room temperature. Crystals appeared within a week and stopped growing after 3 weeks. X-ray diffraction data were collected at beamline P13 at the European Molecular Biology Laboratory (EMBL) outstation at Deutsches Elektronen-Synchrotron, Hamburg, Germany.

Following size exclusion chromatography, the quadruple mutant of GQKV-Fdh_{SNO} was concentrated to 18 mg·mL⁻¹ using a 10 000 MWCO concentrator. The protein was mixed with a custom screen crystallization buffer composed of 0.05 M citric acid pH 4.5, 5–20% PEG 3350 and 0.05–0.1 M MgCl₂. This buffer mixture was predetermined from thermal shift assay results and the protein

mixed with the buffer in a ratio of 2 : 1, respectively. Long, colourless rectangular prism crystals were obtained via the sitting drop vapour diffusion technique which were of suitable quality for X-ray diffraction studies. The crystals were soaked for 20 s in a 0.01 M solution of NADP⁺ and NaN₃ and were then further soaked in 30% (v/v) PEG 400 for cryo-protection. The crystals were subsequently flash-frozen in liquid nitrogen in preparation for diffraction experiments. Data were collected at beam line ID30A-1 (ESRF, Grenoble).

All data were processed with XDS [75]. WT Fdh_{SNO} crystallized in *P1* space group with four molecules in the asymmetric unit, and diffracted to the resolution of 2.1 Å. The structure of apo-Fdh_{PSE} from the Protein Data Bank (PDB entry: 2NAC) was used as a search model for the molecular replacement. A preliminary Fdh_{SNO} model was obtained running the BALBES pipeline [76]. The electron density map was manually inspected and all residues from position 2 to 373 could be unambiguously modelled. GQKV-Fdh_{SNO} diffracted to 2.5 Å resolution (*P6₁* space group), allowing the unambiguous placement of the amino acids 2–382 within the experimental density map. The structure of holo-Fdh_{PSE} from the Protein Data Bank (PDB entry: 2NAD) was used as a search model for Molecular Replacement with Phaser [77]. The model was built using Coot [78], and the refinement and validation steps were carried out with Phenix [79]. Data collection and refinement statistics for all proteins are reported in Table S4. All models were deposited into the PDB repository with the following IDs: 7QZ1 for Fdh_{SNO} and 8OQ2 for GQKV-Fdh_{SNO}.

Acknowledgements

This work was supported by the Dutch Research Council (NWO) Gravitation program (Building a Synthetic Cell), grant No. 024.003.019. NP, AH, and AG received funding from the Horizon 2020 research and innovation program with the Marie Skłodowska Curie grant agreement No. 713482, and from the European Research Council on the Advanced Grant Suprabiotics No. 694610. The authors thank Dr. Patricia Alvarez-Sieiro for the assistance with the codon-optimization of the gene *Snov_3272* (encoding Fdh_{SNO}) in the synthetic gene *synfdh* for the expression in *E. coli*. We acknowledge the use of the DESY (EMBL) synchrotron facility in Hamburg and the support of its staff at the beamline P13. We are grateful to Matthew Bowler at the ESRF for providing assistance in using beamline ID30A-1 (BAG proposal #MX-2407).

Conflict of interest

The authors declare no conflict of interest.

Author contributions

MP and DJS designed the study and wrote the main draft of the manuscript; MP, JJW and JC performed the protein purification and the biochemical assays, and analysed the data; MP and JC designed and carried out site-directed mutagenesis to develop the protein mutants; NP carried out the protein crystallization and resolved the crystallographic structure of the wild-type protein; JJW carried out the protein crystallization and resolved the crystallographic structure of the quadruple mutant protein; MP, JJW, NP, JC, AH, AG and DJS reviewed and contributed to the final version of the manuscript; DJS supervised the work.

Peer review

The peer review history for this article is available at <https://www.webofscience.com/api/gateway/wos/peer-review/10.1111/febs.16871>.

Data availability statement

The atomic coordinates of the wild-type Fdh_{SNO} have been deposited in the Protein Data Bank as entry 7QZ1, the structure of GQKV- Fdh_{SNO} in complex with NADP⁺ and azide is available with the PDB entry 8OQ2. All data and experimental methods are described in the main manuscript and/or the Supporting Information. All data used in the analysis are available upon reasonable request to the lead author.

References

- 1 Yishai O, Lindner SN, Gonzalez de la Cruz J, Tenenboim H & Bar-Even A (2016) The formate bioeconomy. *Curr Opin Chem Biol* **35**, 1–9.
- 2 Cotton CAR, Claassens NJ, Benito-vaquerizo S & Bar-even A (2020) Renewable methanol and formate as microbial feedstocks. *Curr Opin Biotechnol* **62**, 168–180.
- 3 De Luna P, Hahn C, Higgins D, Jaffer SA, Jaramillo TF & Sargent EH (2019) What would it take for renewably powered electrosynthesis to displace petrochemical processes? *Science* **364**, eaav3506.
- 4 Calzadiaz-Ramirez L & Meyer AS (2022) Formate dehydrogenases for CO₂ utilization. *Curr Opin Biotechnol* **73**, 95–100.
- 5 Kim S, Lindner SN, Aslan S, Yishai O, Wenk S & Schann K (2020) Growth of *E. coli* on formate and methanol via the reductive glycine pathway. *Nat Chem Biol* **16**, 538–545.
- 6 Claassens NJ, Sa I, Sousa DZ & Bar-even A (2018) Towards sustainable feedstocks : a guide to electron donors for microbial carbon fixation. *Curr Opin Biotechnol* **50**, 195–205.
- 7 Kim S, Kim MK, Lee SH, Yoon S & Jung KD (2014) Conversion of CO₂ to formate in an electroenzymatic cell using *Candida boidinii* formate dehydrogenase. *J Mol Catal B: Enzym* **102**, 9–15.
- 8 Tishkov VI & Popov VO (2006) Protein engineering of formate dehydrogenase. *Biomol Eng* **23**, 89–110.
- 9 Berríos-Rivera SJ, Bennett GN & San KY (2002) Metabolic engineering of *Escherichia coli*: increase of NADH availability by overexpressing an NAD⁺-dependent formate dehydrogenase. *Metab Eng* **4**, 217–229.
- 10 Ernst M, Kaup B, Müller M, Bringer-Meyer S & Sahm H (2005) Enantioselective reduction of carbonyl compounds by whole-cell biotransformation, combining a formate dehydrogenase and a (R)-specific alcohol dehydrogenase. *Appl Microbiol Biotechnol* **66**, 629–634.
- 11 Rathod J, Dhebar S & Archana G (2017) Efficient approach to enhance whole cell azo dye decolorization by heterologous overexpression of *Enterococcus* sp. L2 azoreductase (azoA) and *Mycobacterium vaccae* formate dehydrogenase (fdh) in different bacterial systems. *Int Biodeter Biodegr* **124**, 91–100.
- 12 Yamamoto H, Mitsuhashi K, Kimoto N, Kobayashi Y & Esaki N (2005) Robust NADH-regenerator: improved α -haloketone-resistant formate dehydrogenase. *Appl Microbiol Biotechnol* **67**, 33–39.
- 13 Zhang Y, Wang Y, Wang S & Fang B (2017) Engineering bi-functional enzyme complex of formate dehydrogenase and leucine dehydrogenase by peptide linker mediated fusion for accelerating cofactor regeneration. *Eng Life Sci* **17**, 989–996.
- 14 Partipilo M, Ewins EJ, Frallicciardi J, Robinson T, Poolman B & Slotboom DJ (2021) Minimal pathway for the regeneration of redox cofactors. *JACS Au* **1**, 2280–2293.
- 15 Popov VO & Lamzin VS (1994) NAD⁺-dependent formate dehydrogenase. *Biochem J* **301**, 625–643.
- 16 Rojkova AM, Galkin AG, Kulakova LB, Serov AE, Savitsky PA, Fedorchuk VV & Tishkov VI (1999) Bacterial formate dehydrogenase. Increasing the enzyme thermal stability by hydrophobization of alpha-helices. *FEBS Lett* **445**, 183–188.
- 17 Slusarczyk H, Felber S, Kula MR & Pohl M (2000) Stabilization of NAD-dependent formate dehydrogenase from *Candida boidinii* by site-directed mutagenesis of cysteine residues. *Eur J Biochem* **267**, 1280–1289.
- 18 Hoelsch K, Sührer I, Heusel M & Weuster-Botz D (2013) Engineering of formate dehydrogenase: synergistic effect of mutations affecting cofactor

- specificity and chemical stability. *Appl Microbiol Biotechnol* **97**, 2473–2481.
- 19 Jiang HW, Chen Q, Pan J, Zheng GW & Xu JH (2020) Rational engineering of formate dehydrogenase substrate/cofactor affinity for better performance in NADPH regeneration. *Appl Biochem Biotechnol* **192**, 530–543.
- 20 Calzadiaz-Ramirez L, Calvó-Tusell C, Stoffel GMM, Lindner SN, Osuna S, Erb TJ, Garcia-Borràs M, Bar-Even A & Acevedo-Rocha CG (2020) In vivo selection for formate dehydrogenases with high efficiency and specificity toward NADP⁺. *ACS Catal* **10**, 7512–7525.
- 21 Hummel W (1999) Large-scale applications of NAD(P)-dependent oxidoreductases: recent developments. *Trends Biotechnol* **17**, 487–492.
- 22 Breuer M, Ditrich K, Habicher T, Hauer B, Keßeler M, Stürmer R & Zelinski T (2004) Industrial methods for the production of optically active intermediates. *Angew Chem Int Ed Engl* **43**, 788–824.
- 23 Hall M & Bommarius AS (2011) Enantioenriched compounds via enzyme-catalyzed redox reactions. *Chem Rev* **111**, 4088–4110.
- 24 Chen BS & Ribeiro de Souza FZ (2019) Enzymatic synthesis of enantiopure alcohols: current state and perspectives. *RSC Adv* **9**, 2102–2115.
- 25 Abdelraheem EMM, Busch H, Hanefeld U & Tonin F (2019) Biocatalysis explained: from pharmaceutical to bulk chemical production. *React Chem Eng* **4**, 1878–1894.
- 26 Wu S, Snajdrova R, Moore JC, Baldenius K & Bornscheuer UT (2021) Biocatalysis: enzymatic synthesis for industrial applications. *Angew Chem Int Ed Engl* **60**, 88–119.
- 27 Nanba H, Takaoka Y & Hasegawa J (2003) Purification and characterization of an α -haloketone-resistant formate dehydrogenase from *Thiobacillus* sp. strain KNK65MA, and cloning of the gene. *Biosci Biotechnol Biochem* **67**, 2145–2153.
- 28 Tishkov VI & Popov VO (2004) Catalytic mechanism and application of formate dehydrogenase. *Biochemistry* **69**, 1252–1267.
- 29 Tishkov VI, Galkin AG, Marchenko GN, Egorova OA, Sheluho DV, Kulakova LB, Dementieva LA & Egorov AM (1993) Catalytic properties and stability of a *Pseudomonas* sp.101 formate dehydrogenase mutants containing Cys-255-Ser and Cys-255-met replacements. *Biochem Biophys Res Commun* **192**, 976–981.
- 30 Schütte H, Flossdorf J, Sahm H & Kula M-R (1976) Purification and properties of formaldehyde dehydrogenase and formate dehydrogenase from *Candida boidinii*. *Eur J Biochem* **62**, 151–160.
- 31 Avilova TV, Egorova OA, Ioanesyan LS & Egorov AM (1985) Biosynthesis, isolation and properties of NAD-dependent formate dehydrogenase from the yeast *Candida methylca*. *Eur J Biochem* **152**, 657–662.
- 32 Asano Y, Sekigawa T, Inukai H & Nakazawa A (1988) Purification and properties of formate dehydrogenase from *Moraxella* sp. strain C-1. *J Bacteriol* **170**, 3189–3193.
- 33 Nanba H, Takaoka Y & Hasegawa J (2003) Purification and characterization of formate dehydrogenase from *Ancylobacter aquaticus* strain KNK607M, and cloning of the gene. *Biosci Biotechnol Biochem* **67**, 720–728.
- 34 Kappler U, Davenport K, Beatson S, Lucas S, Lapidus A, Copeland A, Berry KW, Del Rio TG, Hammon N, Dalin E *et al.* (2012) Complete genome sequence of the facultatively chemolithoautotrophic and methylotrophic alpha Proteobacterium *Starkeya novella* type strain (ATCC 8093T). *Stand Genomic Sci* **7**, 44–58.
- 35 Casadaban MJ & Cohen SN (1980) Analysis of gene control signals by DNA fusion and cloning in *Escherichia coli*. *J Mol Biol* **138**, 179–207.
- 36 Privalov PL (1990) Cold denaturation of protein. *Crit Rev Biochem Mol Biol* **25**, 281–306.
- 37 Blundell TL & Jenkins JA (1977) The binding of heavy metals to proteins. *Chem Soc Rev* **6**, 139–171.
- 38 Falchuk KH, Goldwater LJ & Vallee BL (1977) The biochemistry and toxicology of mercury. *Chem Mercur* **259**–283.
- 39 Law MR, Wald NJ & ARR (2003) Quantifying effects of statins on low density lipoprotein cholesterol, ischaemic heart disease, and stroke: systematic review and meta-analysis. *BMJ* **326**, 1423–1420.
- 40 Ma SK, Gruber J, Davis C, Newman L, Gray D, Wang A, Grate J, Huisman GW & Sheldon RA (2010) A green-by-design biocatalytic process for atorvastatin intermediate. *Green Chem* **12**, 81–86.
- 41 Rao ST & Rossmann MG (1973) Comparison of super-secondary structures in proteins. *J Mol Biol* **76**, 241–256.
- 42 Lamzin VS, Dauter Z, Popov VO, Harutyunyan EH & Wilson KS (1994) High resolution structures of holo and apo formate dehydrogenase. *J Mol Biol* **236**, 759–785.
- 43 Kumar S (2010) Engineering cytochrome P450 biocatalysts for biotechnology, medicine and bioremediation. *Expert Opin Drug Metab Toxicol* **6**, 115–131.
- 44 Kamerbeek NM, Fraaije MW & Janssen DB (2004) Identifying determinants of NADPH specificity in Baeyer-Villiger monooxygenases. *Eur J Biochem* **271**, 2107–2116.
- 45 Gul-karaguler N, Sessions RB, Clarke AR & Holbrook JJ (2001) A single mutation in the NAD specific FDH from *Candida* allows to use NADP. *Biotechnol Lett* **23**, 283–287.
- 46 Serov AE, Popova AS, Fedorchuk VV & Tishkov VI (2002) Engineering of coenzyme specificity of formate

- dehydrogenase from *Saccharomyces cerevisiae*. *Biochem J* **367**, 841–847.
- 47 Hatrongjit R & Packdibamrung K (2010) A novel NADP⁺-dependent formate dehydrogenase from *Burkholderia stabilis* 15516: screening, purification and characterization. *Enzyme Microb Technol* **46**, 557–561.
 - 48 Fogal S, Beneventi E, Cendron L & Bergantino E (2015) Structural basis for double cofactor specificity in a new formate dehydrogenase from the acidobacterium *Granulicella mallensis* MP5ACTX8. *Appl Microbiol Biotechnol* **99**, 9541–9554.
 - 49 Kappler U & Nouwens AS (2013) Metabolic adaptation and trophic strategies of soil bacteria-C1-metabolism and sulfur chemolithotrophy in *Starkeya novella*. *Front Microbiol* **4**, 1–12.
 - 50 Sun L, Zhu S, Yang Z, Chen Q, Liu H, Zhang J, Hu G, Li S & Hong Q (2016) Degradation of monocrotophos by *Starkeya novella* YW6 isolated from paddy soil. *Environ Sci Pollut Res* **23**, 3727–3735.
 - 51 d'Errico G, Aloj V, Ventorino V, Bottiglieri A, Comite E, Ritieni A, Marra R, Censi SB, Flematti GR, Pepe O *et al.* (2020) Methyl t-butyl ether-degrading bacteria for bioremediation and biocontrol purposes. *PLoS One* **15**, 1–16.
 - 52 Bosma EF, Van Der OJ, De VWM & Van KR (2013) Sustainable production of bio-based chemicals by extremophiles. *Curr Biotechnol* **999**, 5–6.
 - 53 Mishra S, Lin Z, Pang S, Zhang W, Bhatt P & Chen S (2021) Recent advanced technologies for the characterization of xenobiotic-degrading microorganisms and microbial communities. *Front Bioeng Biotechnol* **9**, 632059.
 - 54 Whitman WB, Coleman DC & Wiebe WJ (1998) Prokaryotes: the unseen majority. *Proc Natl Acad Sci U S A* **95**, 6578–6583.
 - 55 Gans J, Wolinsky M & Dunbar J (2005) Computational improvements reveal great bacterial diversity and high toxicity in soil. *Science* **309**, 1387–1390.
 - 56 Uchiyama T & Miyazaki K (2009) Functional metagenomics for enzyme discovery: challenges to efficient screening. *Curr Opin Biotechnol* **20**, 616–622.
 - 57 Lee MH & Lee S-W (2013) Bioprospecting potential of the soil metagenome: novel enzymes and bioactivities. *Genomics Inform* **11**, 114–120.
 - 58 Iraneta PC & Byrd S Best practices for maintaining column performance in size-exclusion chromatography during long-term storage.
 - 59 Bandaria JN, Dutta S, Hill SE, Kohen A & Cheatum CM (2008) Fast enzyme dynamics at the active site of formate dehydrogenase. *J Am Chem Soc* **130**, 22–23.
 - 60 Tchertanov L (2000) Understanding the peculiarities of azide and thiocyanate binding in proteins: use of the small molecule structural data. *Supramol Chem* **12**, 67–91.
 - 61 Hartmann T, Schwanhold N & Leimk S (2015) Assembly and catalysis of molybdenum or tungsten-containing formate dehydrogenases from bacteria. *Biochim Biophys Acta Proteins Proteom* **1854**, 1090–1100.
 - 62 Mielke T, Teutloff C, Duffus BR, Bürger J, Hartmann T, Leimkühler S & Wendler P (2020) Cryo-EM structures reveal intricate Fe-S cluster arrangement and charging in *Rhodobacter capsulatus* formate dehydrogenase. *Nat Commun* **11**, 1–9.
 - 63 Partipilo M, Claassens NJ & Slotboom DJ (2023) A Hitchhiker's guide to supplying enzymatic reducing power into synthetic cells. *ACS Synth Biol* **12**, 947–962.
 - 64 Zhu D, Mukherjee C & Hua L (2005) “Green” synthesis of important pharmaceutical building blocks: enzymatic access to enantiomerically pure α -chloroalcohols. *Tetrahedron Asymmetry* **16**, 3275–3278.
 - 65 Tokoshima D, Hanaya K, Shoji M & Sugai T (2013) Whole-cell yeast-mediated preparation of (R)-2-chloro-1-(3-nitrophenyl) ethanol as a synthetic precursor for (R)-phenylephrine. *J Mol Catal B: Enzym* **97**, 95–99.
 - 66 Zhao JW, Wu HL, Zhang JD, Gao WC, Fan XJ, Chang HH, Wei WL & Xu JH (2018) One pot simultaneous preparation of both enantiomer of β -amino alcohol and vicinal diol via cascade biocatalysis. *Biotechnol Lett* **40**, 349–358.
 - 67 Alcalde M, Ferrer M & Plou FJ (2006) Environmental biocatalysis: from remediation with enzymes to novel green processes. *Biocatal Biotransformation* **24**, 281–287.
 - 68 Verma S & Kuila A (2019) Bioremediation of heavy metals by microbial process. *Environ Technol Innov* **14**, 100369.
 - 69 Chen W, Brühlmann F, Richins RD & Mulchandani A (1999) Engineering of improved microbes and enzymes for bioremediation. *Curr Opin Biotechnol* **10**, 137–141.
 - 70 Nakamura Y, Gojobori T & Ikemura T (2000) Codon usage tabulated from international DNA sequence databases: status for the year 2000. *Nucleic Acids Res* **28**, 292.
 - 71 Geertsma ER & Dutzler R (2011) A versatile and efficient high-throughput cloning tool for structural biology. *Biochemistry* **50**, 3272–3278.
 - 72 Huynh K & Partch CL (2015) Analysis of protein stability and ligand interactions by thermal shift assay. *Curr Protoc Protein Sci* **79**, 28.9.1–28.9.14.
 - 73 Walmsley TA, Abernethy MH & Fitzgerald HP (1987) Effect of daylight on the reaction of thiols with Ellman's reagent, 5,5'-dithiobis(2-nitrobenzoic acid). *Clin Chem* **33**, 1928–1931.
 - 74 Han K, Delacourte A & Hemon B (1987) Chemical modification of thiol group(s) in protein: application to the study of anti-microtubular drugs binding. *Comp Biochem Physiol B* **88**, 1057–1065.
 - 75 Kabsch W (2010) Xds. *Acta Crystallogr D* **66**, 125–132.

- 76 Long F, Vagin AA, Young P & Murshudov GN (2007) BALBES: a molecular-replacement pipeline. *Acta Crystallogr D* **64**, 125–132.
- 77 McCoy AJ, Grosse-Kunstleve RW, Adams PD, Winn MD, Storoni LC & Read RJ (2007) Phaser crystallographic software. *J Appl Cryst* **40**, 658–674.
- 78 Emsley P & Cowtan K (2004) Coot: model-building tools for molecular graphics. *Acta Crystallogr D* **60**, 2126–2132.
- 79 Adams PD, Afonine PV, Bunkóczi G, Chen VB, Davis IW, Echols N, Headd JJ, Hung LW, Kapral GJ, Grosse-Kunstleve RW *et al.* (2010) PHENIX: a comprehensive Python-based system for macromolecular structure solution. *Acta Crystallogr D* **66**, 213–221.

Supporting information

Additional supporting information may be found online in the Supporting Information section at the end of the article.

Table S1. Amino acid occurrence in three positions of close homologues of Fdh_{TBA}.

Table S2. Genomic GC content comparison.

Table S3. Codon-optimization for the expression in *E. coli* of the gene *Snov_3272* from *S. novella*.

Table S4. Data collection and refinement statistics of apo- and holo-Fdh from *Starkeya novella*, PDB entry: [7QZ1](#) and [8OQ2](#), respectively.

Table S5. List and main features of the available structures of NAD(P)⁺-dependent Fdhs.

Table S6. Accessible Surface Area and Accessibility calculations of positions displaying cysteines from the crystal structures of Fdh_{SNO}, Fdh_{PSE} and Fdh_{CBO}.

Table S7. List of the primers used in this study.

Fig. S1. Codon-optimization for the recombinant overproduction of Fdh_{SNO}.

Fig. S2. NAD⁺-specificity of Fdh_{SNO}.

Fig. S3. *IC*₅₀ plots for azide (N₃) and thiocyanate (SCN).

Fig. S4. Size-exclusion chromatography (SEC) on a Superdex 200 Increase 10/300 GL of the cysteine mutants of Fdh_{SNO} following Immobilized Metal Affinity Chromatography.

Fig. S5. Chemical stability of WT Fdh_{SNO} and V255C against ethyl 4-chloroacetate (ECAA) and ethyl (S)-(–)-4-chloro-3-hydroxybutyrate (ECHB).

Fig. S6. Size-exclusion chromatography (SEC) on a Superdex 200 Increase 10/300 GL column of the mutants of Fdh_{SNO} following Immobilized Metal Affinity Chromatography.

Fig. S7. Kinetic data for NADP⁺-dependent Fdh_{SNO} constructs D221Q and GQKV.

Fig. S8. Conservation of the hydrogen-bond network formed between azide and active site residues in different Fdhs.